BRAIN COMMUNICATIONS

Nigral diffusivity, but not free water, correlates with iron content in Parkinson's disease

Jason Langley,[1] Daniel E. Huddleston[2] and Xiaoping Hu[1,3]

The loss of melanized neurons in the substantia nigra pars compacta is a primary feature in Parkinson's disease. Iron deposition occurs in conjunction with this loss. Loss of nigral neurons should remove barriers for diffusion and increase diffusivity of water molecules in regions undergoing this loss. In metrics from single-compartment diffusion tensor imaging models, these changes should manifest as increases in mean diffusivity and reductions in fractional anisotropy as well as increases in the free water compartment in metrics derived from bi-compartment models. However, studies examining nigral diffusivity changes from Parkinson's disease with single-compartment models have yielded inconclusive results and emerging evidence in control subjects indicates that iron corrupts diffusivity metrics derived from single-compartment models. We aimed to examine Parkinson's disease-related changes in nigral iron and diffusion measures from single- and bi-compartment models as well as assess the effect of iron on these diffusion measures in two separate Parkinson's cohorts. Iron-sensitive data and diffusion data were analysed in two cohorts: First, a discovery cohort consisting of 71 participants (32 control participants and 39 Parkinson's disease participants) was examined. Second, an external validation cohort, obtained from the Parkinson's Progression Marker's Initiative, consisting of 110 participants (58 control participants and 52 Parkinson's disease participants) was examined. The effect of iron on diffusion measures from single- and bi-compartment models was assessed in both cohorts. Measures sensitive to the free water compartment (discovery cohort: $P = 0.006$; external cohort: $P = 0.01$) and iron content (discovery cohort: $P < 0.001$; validation cohort: $P = 0.02$) were found to increase in substantia nigra of the Parkinson's disease group in both cohorts. However, diffusion markers derived from the single-compartment model (i.e. mean diffusivity and fractional anisotropy) were not replicated across cohorts. Correlations were seen between single-compartment diffusion measures and iron markers in the discovery cohort (iron-mean diffusivity: $r = -0.400$, $P = 0.006$) and validation cohort (iron-mean diffusivity: $r = -0.387$, $P = 0.003$) but no correlation was observed between a measure from the bi-compartment model related to the free water compartment and iron markers in either cohort. In conclusion, the variability of nigral diffusion metrics derived from the single-compartment model in Parkinson's disease may be attributed to competing influences of increased iron content, which tends to drive diffusivity down, and increases in the free water compartment, which tends to drive diffusivity up. In contrast to diffusion metrics derived from the single-compartment model, no relationship was seen between iron and the free water compartment in substantia nigra.

1 Center for Advanced Neuroimaging, University of California Riverside, Riverside, CA 92521, USA
2 Department of Neurology, Emory University, Atlanta, GA 30322, USA
3 Department of Bioengineering, University of California Riverside, Riverside, CA 92521, USA

Correspondence to: Xiaoping Hu, PhD
Provost Fellow, Professor and Chair, University of California Riverside
Riverside, CA 92521, USA
E-mail: xhu@engr.ucr.edu

Received June 30, 2021. Revised August 18, 2021. Accepted September 20, 2021. Advance Access publication October 23, 2021

Keywords: Parkinson's disease; substantia nigra pars compacta; diffusion tensor imaging; neuromelanin-sensitive MRI; iron

Abbreviations: ANCOVA = analysis of covariance; AD = axial diffusivity; DTI = diffusion tensor imaging; FA = fractional anisotropy; FW = free water; MD = mean diffusivity; PPMI = Parkinson's Progression Markers Initiative; RD = radial diffusivity; ROI = region of interest; SNpc = substantia nigra pars compacta; TSE = turbo-spin echo; UPDRS-III = Unified Parkinson's Disease Rating Scale Part III

Graphical Abstract

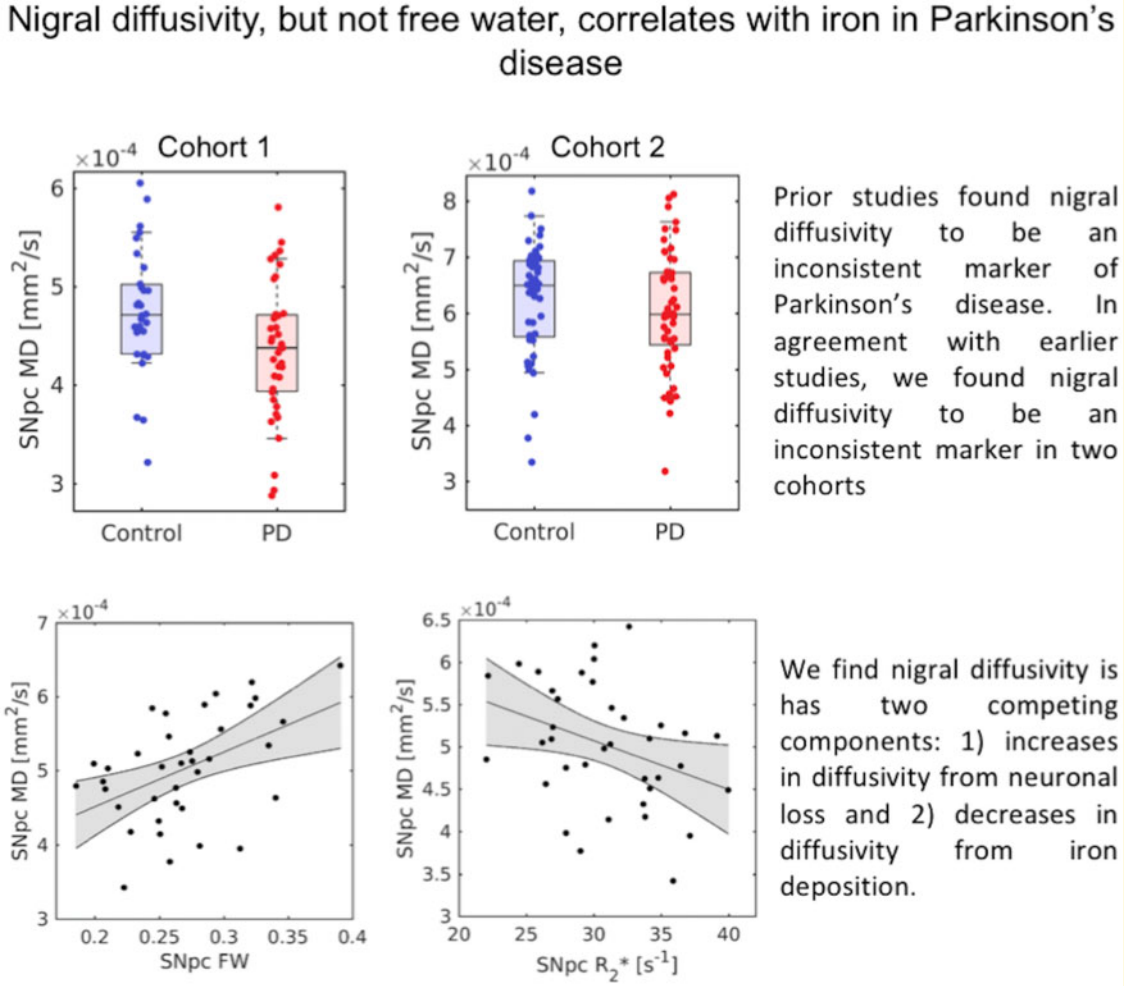

Introduction

Parkinson's disease is a progressive neurodegenerative disorder characterized by resting tremor, bradykinesia, rigidity and gait impairment and affects ~1% of the population over the age of 60 years.[1] Depigmentation of melanized neurons in substantia nigra pars compacta (SNpc) is a primary feature of Parkinson's disease with SNpc undergoing extensive loss of melanized neurons in the early stages of the disease[2,3] and iron is deposited in SNpc concurrently with the loss of melaninzed neurons.[4–6] The loss of melanized neurons should affect SNpc microstructure by removing barriers to diffusion and these microstructural differences can be examined *in vivo* with diffusion imaging, which measures the movement of molecular water.[7]

Diffusion tensor imaging (DTI) is sensitive to the diffusivity of water and allows researchers to probe the directionality of diffusion, known as fractional anisotropy (FA), and the extent of diffusion, known as mean diffusivity (MD), in tissue. Several studies have attempted to use DTI to characterize the effects of Parkinson's disease on SNpc microstructure.[8–14] However, no consensus has emerged from results in prior studies where lower nigral FA[10–13,15] or no difference in nigral FA[8,16–19] have been reported. This inconsistency has hampered the search for diagnostic and progression imaging markers of Parkinson's disease.[17]

While the use of standard (single-compartment) DTI has not yielded reproducible diagnostic biomarkers in SNpc, multi-compartment modelling approaches have yielded consistent diagnostic imaging markers of Parkinson's

disease. In particular, the application of a bi-compartment model has reliably found increases in the CSF volume fraction [free water (FW) compartment] in SNpc of Parkinson's disease as compared to controls.[20–23] Other modelling approaches have revealed Parkinson's disease associated increases in SNpc kurtosis,[24] as well as a reduction in neurite density in Parkinson's disease using the three-compartment neurite orientation dispersion and density imaging model.[25]

Iron is deposited in SNpc after onset of Parkinson's disease.[11,12,26–33] Iron deposition in SNpc may alter diffusivity in the single-compartment model, contributing to the inconsistency of Parkinson's disease DTI imaging markers. Iron has been found to negatively bias diffusivity and positively bias FA in subcortical grey matter structures of older healthy adults.[34,35] While emerging evidence indicates that iron and metrics from a single-compartment diffusion model are correlated, the effect of iron on metrics derived from multi-compartment models is unknown.

In this work, we use an atlas constructed from magnetization transfer-effects, which are sensitive to neuromelanin,[36–39] to localize SNpc and examine Parkinson's disease-related microstructural changes in SNpc using single and multi-compartment models in two cohorts. We further examine the influence of Parkinson's disease-related microstructural and compositional changes on diffusion metrics with the goal of elucidating the variability observed in nigral microstructural measures from earlier studies examining microstructural changes in Parkinson's disease.

Materials and methods

Subjects

Two cohorts were used in this analysis, a discovery cohort and a replication cohort. A total of 92 participants (52 participants with Parkinson's disease and 40 control participants) enrolled in the discovery cohort. Data from 13 Parkinson's disease and 8 control participants were excluded due to motion artefacts or incomplete scans. The final sample size for the discovery cohort was 71 subjects (39 Parkinson's disease participants and 32 control participants). Participants with Parkinson's disease were recruited from the Emory University Movement Disorders Clinic and clinically diagnosed with Parkinson's disease according to the Movement Disorders Society consensus diagnostic criteria.[40] Parkinson's disease patients had early to moderate disease with a Unified Parkinson's Disease Rating Scale Part III (UPDRS-III) ON medications motor score of $\leq$25. Control subjects were recruited from a cohort of individuals without major neurological diagnoses followed by the Emory Alzheimer's Disease Research Center. Specific exclusion criteria included the following: (i) patients showing symptoms or signs of secondary or atypical parkinsonism[41]; (ii) controls were excluded if they scored $\leq$26 on the Montreal Cognitive Assessment indicating cognitive impairment; (iii) any history of vascular territorial stroke, epilepsy, multiple sclerosis, neurodegenerative disease (aside from Parkinson's disease), peripheral neuropathy with motor deficits, parenchymal brain tumour, hydrocephalus or schizophrenia; (iv) treatment with an antipsychotic drug (other than quetiapine at a dose $<$200 mg daily); or (v) if there were any contraindications to MRI imaging. All subjects participating in the discovery cohort gave written informed consent in accordance with local institutional review board regulations.

Demographic information including gender, age and education, was collected for each subject in the discovery cohort. Participants in both the Parkinson's disease and control groups underwent UPDRS-III examination by a fellowship-trained movement disorders neurologist. Parkinson's disease patients were examined and underwent imaging in the ON medication state.

A second cohort was obtained from the Parkinson's Progression Markers Initiative (PPMI) database (www.ppmi-info.org/data). PPMI is a multi-site study collecting imaging, biomarker and clinical assessments in a group of *de novo* Parkinson's disease patients. For up-to-date information on the study, visit www.ppmi-info.org. Full inclusion and exclusion criteria for enrolment in PPMI can be found at the PPMI website (www.ppmi-info.org). Institutional IRB approved the study for each site and subjects gave written informed consent. Criteria for inclusion for subjects from the PPMI database used in this analysis were as follows: (i) participants must be scanned with cardiac-gated DTI and dual echo turbo-spin echo (TSE) acquisitions; and (ii) Parkinson's disease participants must have DTI and dual echo TSE scans at the 48-month time point with scan parameters matching those in the PPMI imaging protocol.

In the PPMI cohort, data from 228 participants (101 Parkinson's disease and 127 control participants) were downloaded in December of 2019. A total of 41 Parkinson's disease and 67 controls were excluded due to inconsistent scan parameters from the DTI or dual echo TSE acquisitions. After triage, eight Parkinson's disease participants and two control participants were excluded due to motion artefacts in the DTI or dual echo TSE acquisitions. The final sample size for the PPMI cohort was 110 (58 control and 52 Parkinson's disease participants). A flow chart summarizing the calculation of the final sample size in both cohorts is shown in Fig. 1.

Image acquisition

Imaging data for the discovery cohort were acquired at Emory University on a 3 T MRI scanner (Prisma Fit, Siemens Healthineers, Malvern, PA) using a 64 channel receive only coil. Images from a T_1-weighted Magnetization Prepared - RApid Gradient Echo (MP-RAGE) sequence [echo time (TE)/repetition time (TR)/inversion time (TI) = 3.02/2600/800 ms, flip angle = 8°,

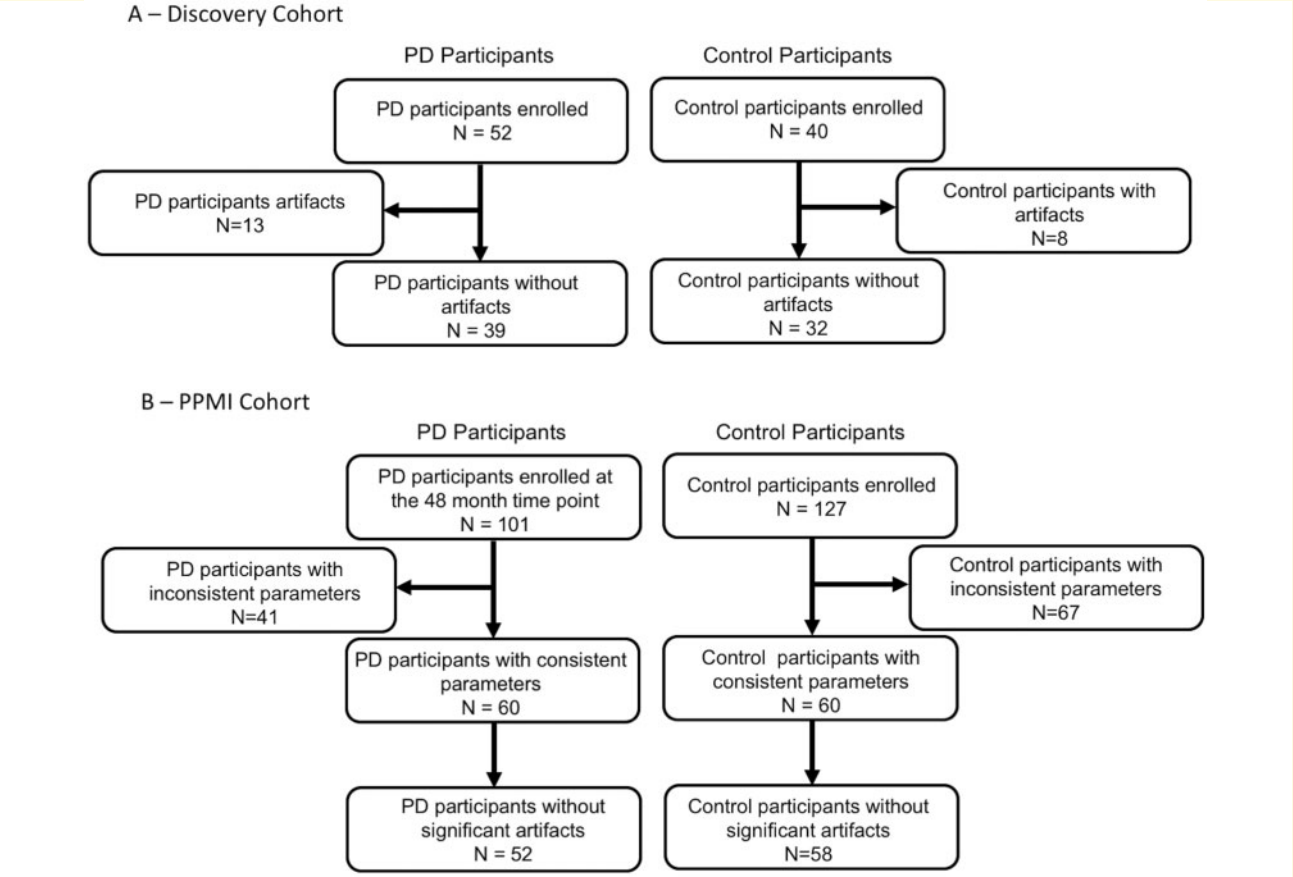

Figure 1 Participant flow chart for both cohorts. (**A**) Participant flow chart for the discovery cohort. (**B**) Participant flow chart for the PPMI cohort.

voxel size = $0.8 \times 0.8 \times 0.8$ mm^3] were used for registration from subject space to common space. Multiecho T_2*-weighted data were collected with a six echo 3 D gradient recalled echo (GRE) sequence: $TE_1/\Delta TE/TR = 4.92/4.92/50$ ms, FOV = 220×220 mm^2, matrix size of $448 \times 336 \times 80$, in-plane resolution = 0.49×0.49 mm^2, slice thickness = 1 mm and (GeneRalized Autocalibrating Partial Parallel Acquisition) GRAPPA acceleration factor = 2.

Diffusion-MRI data in the discovery cohort were collected using a diffusion-weighted spin-echo EPI sequence with parameters matching the Lifespan Human Connectome Project: TE/TR = 89.2/3222 ms, FOV = 210×210 mm^2, matrix size = 140×140, voxel size = $1.5 \times 1.5 \times 1.5$ mm^3, partial Fourier = 6/8 and multiband factor = 4, with 92 slices. Six images without diffusion weighting ($b = 0$ s/mm^2) were also acquired with matching parameters. Monopolar diffusion encoding gradients were applied in 99 directions with b values of 1000 and 2000 s/mm^2. Two sets of diffusion-weighted images with phase-encoding directions of opposite polarity were acquired to correct for susceptibility distortion.[42]

T_1-weighted structural images in the PPMI cohort were acquired with an MP-RAGE sequence (TE/TR/TI = 2.98/2300/900 ms, flip angle = 9.0° and voxel size = $1 \times 1 \times 1$ mm^3) were acquired for registration to common space. Dual echo TSE images were acquired with the following parameters: $TE_1/TE_2/TR = 11/101/3270$ ms; FOV = 240×213 mm^2; voxel size = $0.9 \times 0.9 \times 3$ mm^3; 48 slices. Cardiac-gated diffusion-MRI data in the PPMI cohort were acquired using a monopolar diffusion encoding gradient with 64 unique gradient directions and the following parameters: TE/TR = 88/650–1100 ms, flip angle = 90.0°, FOV = 229×229 mm^2, voxel size = $1.98 \times 1.98 \times 2$ mm^3, b value of 1000 s/mm^2, cardiac-triggered, with 72 slices.

DTI processing

For both cohorts, diffusion data were preprocessed with (the FMRIB Software Library) FSL.[43–45] In the discovery cohort, magnetic field inhomogeneities were estimated from $b = 0$ images with phase-encoding gradients of opposite polarity. Susceptibility induced distortions, motion and eddy-current induced distortions were corrected by EDDY. In the PPMI cohort, diffusion MR data were corrected for motion and eddy-current distortions using EDDY in FSL. Next, susceptibility distortions were reduced by non-linearly fitting the $b = 0$ image to second echo from the TSE acquisition. For both cohorts,

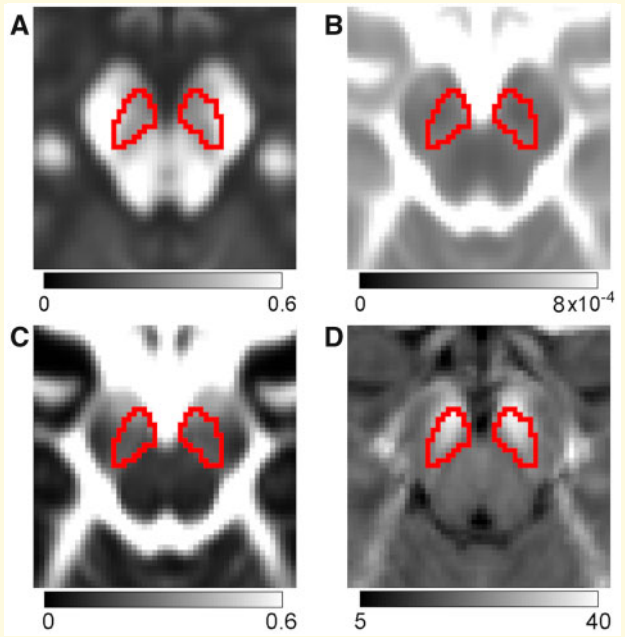

Figure 2 Illustration of the SNpc ROI used in this analysis. The SNpc ROI is outlined on mean SNpc FA (**A**), mean SNpc MD (**B**) and mean FW (**C**) and R_2* (**D**) images from the control group of the discovery cohort. For purposes of visualization, each participant's image (FA, MD, FW and R_2*) was transformed to MNI 1 mm space and averaged.

parameters derived from the diffusion data were estimated using DTIFIT. A bi-compartment model,[46] implemented in DIPY,[47] was used to construct FW maps in both cohorts.

For subjects in both cohorts, the $b = 0$ image was brain extracted[48] and registered to the brain extracted T_1-weighted image using a rigid body transform with a boundary-based registration cost function.

Iron processing

For both cohorts, R_2* (from multiecho GRE acquisition) or R_2 (from multiecho TSE acquisition) values were estimated using a custom script in MATLAB by fitting a monoexponential model to the multiecho GRE or multiecho TSE images. The resulting R_2* or R_2 maps were aligned to the T_1-weighted image using a rigid body transform derived via the magnitude image from the first echo.

Transformation of SNpc region of interests

A SNpc atlas, derived from magnetization-transfer images in a cohort of 76 healthy older participants (aged 66.6 years ± 6.4 years), was used as a region of interest (ROI) in the diffusion and iron analyses.[49] The SNpc atlas was transformed from Montreal Neurological Institute (MNI) common space to subject space using linear and non-linear transforms in FSL[45,50] as previously described.[34] Mean DTI and iron measures (discovery cohort: R_2*, FA, MD and FW; PPMI cohort: R_2, FA, MD and FW) were calculated in the SNpc for each subject. Figure 2 shows the SNpc ROI overlaid on mean SNpc FA, mean SNpc MD and mean SNpc FW images from the control group in discovery cohort.

Statistical analysis

Statistical analyses were performed using SPSS version 24 (IBM SPSS Statistics, Chicago, IL, USA). Quantitative data are expressed as mean ± standard deviation. Group differences in both cohorts were assessed using between-group t-tests. A one-tailed *t*-test with a significance level of $P = 0.05$ was used for group comparisons of iron measures (R_2* and R_2) and we hypothesize an increase in mean SNpc iron measures will be observed in the Parkinson's disease group since histopathology and imaging studies in Parkinson's disease have noted an increase in SNpc iron.[6,26,51] A one-tailed *t*-test with a significance level of $P = 0.05$ was used for group comparisons of diffusion measures from a single-compartment model [MD, radial diffusivity (RD) and FA]. We expect SNpc diffusivity will be reduced and SNpc FA will be increased in the Parkinson's disease group since earlier studies have noted that diffusivity (MD and RD) and FA are negatively and positively biased, respectively, by iron deposition.[34,52] A one-tailed *t*-test with a significance level of $P = 0.05$ was used for group comparisons of nigral FW measures since prior imaging studies found elevated FW in the substantia nigra of Parkinson's disease patients as compared to controls.[21,22] We hypothesize that measures of FW will be increased in the Parkinson's disease group of both cohorts.

SNpc diffusivity and FA are correlated with iron measures.[34,52] A *post hoc* analysis of covariance (ANCOVA) was performed to remove the influence of iron in these measures and evaluate Parkinson's disease-related microstructural changes in SNpc without contributions from iron. To assess the impact of Parkinson's disease severity on imaging biomarkers, clinical measures (UPDRS-III ON score and disease duration) were correlated with mean SNpc diffusion indices as well as with mean SNpc iron. A correlation was considered to be significant if $P < 0.05$.

Data availability

The data from the discovery cohort that support the findings of this study are available from the corresponding author, upon reasonable request. Data from the PPMI cohort can be obtained from the PPMI database (www.ppmi-info.org/data).

Table 1 Subject demographics and clinical information subjects used in both cohorts

Variable	Discovery cohort			PPMI cohort		
	CO ($n = 32$)	Parkinson's ($n = 39$)	*P*-value	CO ($n = 58$)	Parkinson's ($n = 52$)	*P*-value
Gender (M/F)	12/20	20/19	0.07	40/18	33/19	0.21
Age (years)	65.5 ± 9.2	63.7 ± 10.2	0.41	61.7 ± 10.9	63.2 ± 9.9	0.45
Education (years)	14.4 ± 6.0	15.1 ± 4.7	0.57	16.0 ± 3.0	15.4 ± 2.9	0.26
UPDRS-III ON score	2.6 ± 2.2	24.0 ± 11.4	$<10^{-4}$	0.8 ± 1.3	18.5 ± 12.6	$<10^{-4}$
Disease duration (years)		4.0 ± 3.6			4.6 ± 0.6	

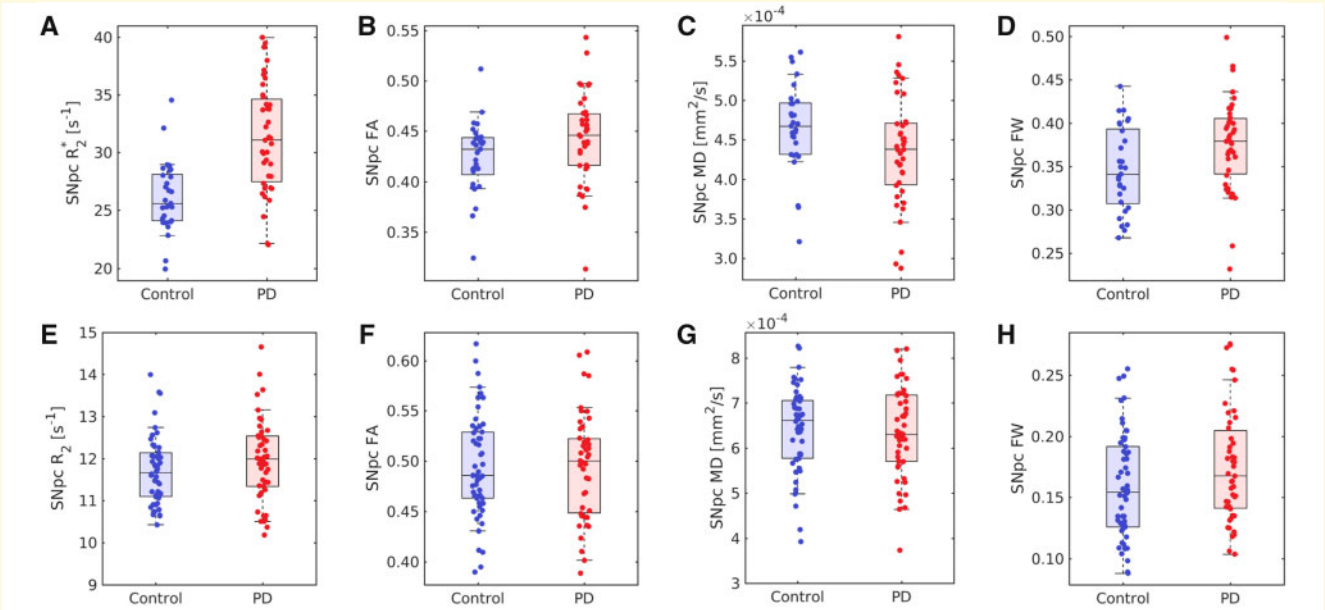

Figure 3 Group comparisons for both cohorts. Comparisons of R_2^* ($P < 0.001$), FA ($P = 0.001$), MD ($P = 0.001$) and FW ($P = 0.001$) in the discovery cohort are shown in **A–D**, respectively. The bottom row (**E–H**) show group comparisons for R_2 ($P = 0.023$), FA ($P = 0.371$), MD ($P = 0.330$) and FW ($P = 0.01$), respectively, in the PPMI cohort. In all box plots, the top and bottom of the box denote the 25th and 75th percentiles, respectively, with the line denoting the median value.

Results

No differences were observed in gender (discovery: $P = 0.07$; PPMI: $P = 0.21$), age (discovery: $P = 0.41$; PPMI: $P = 0.45$) or education (discovery: $P = 0.57$; PPMI: $P = 0.26$) in either cohort. Demographic information for participants in both cohorts is summarized in Table 1.

In the discovery cohort, results revealed a reduction in SNpc MD (Parkinson's: 4.40×10^{-4} $mm^2/s \pm 7.3 \times 10^{-5}$ mm^2/s; control: 4.72×10^{-4} $mm^2/s \pm 4.8 \times 10^{-5}$ mm^2/s; $P = 0.017$; $t = 2.0$) and SNpc RD (Parkinson's: 3.33×10^{-4} $mm^2/s \pm 6.6 \times 10^{-5}$ mm^2/s; control: 3.61×10^{-4} $mm^2/s \pm 5.1 \times 10^{-5}$ mm^2/s; $P = 0.022$; $t = 2.0$) in the Parkinson's disease group relative to the control group. An increase in SNpc FA was seen in the Parkinson's disease group as compared to the control group (Parkinson's: 0.44 ± 0.05; control: 0.42 ± 0.03; $P = 0.044$; $t = -2.0$). No significant difference was observed in SNpc axial diffusivity (AD) (Parkinson's: 6.60×10^{-4} $mm^2/s \pm 9.4 \times 10^{-5}$ mm^2/s; control: 6.92×10^{-4} $mm^2/s \pm 8.2 \times 10^{-5}$ mm^2/s; $P = 0.065$; $t = 1.5$) between groups. Bi-compartment analysis revealed an increase in the SNpc FW compartment of Parkinson's patients as compared to controls (Parkinson's: 0.27 ± 0.04; control: 0.23 ± 0.05; $P = 0.006$; $t = 2.6$). An increase in mean SNpc R_2^* was seen in the Parkinson's disease group as compared to the control group (Parkinson's: $31.3 \pm 4.4\ s^{-1}$; control: $26.0 \pm 3.0\ s^{-1}$; $P < 0.001$; $t = 5.429$).

In the PPMI cohort, no significant differences were seen in SNpc FA (Parkinson's: 0.49 ± 0.06; control: 0.49 ± 0.05; $P = 0.371$; $t = 0.329$), SNpc MD (Parkinson's: 6.51×10^{-4} $mm^2/s \pm 1.11 \times 10^{-4}$ mm^2/s; control: 6.40×10^{-4} $mm^2/s \pm 1.24 \times 10^{-4}$ mm^2/s; $P = 0.330$; $t = -0.441$), SNpc RD (Parkinson's: 4.86×10^{-4} $mm^2/s \pm 1.20 \times 10^{-4}$ mm^2/s; control:

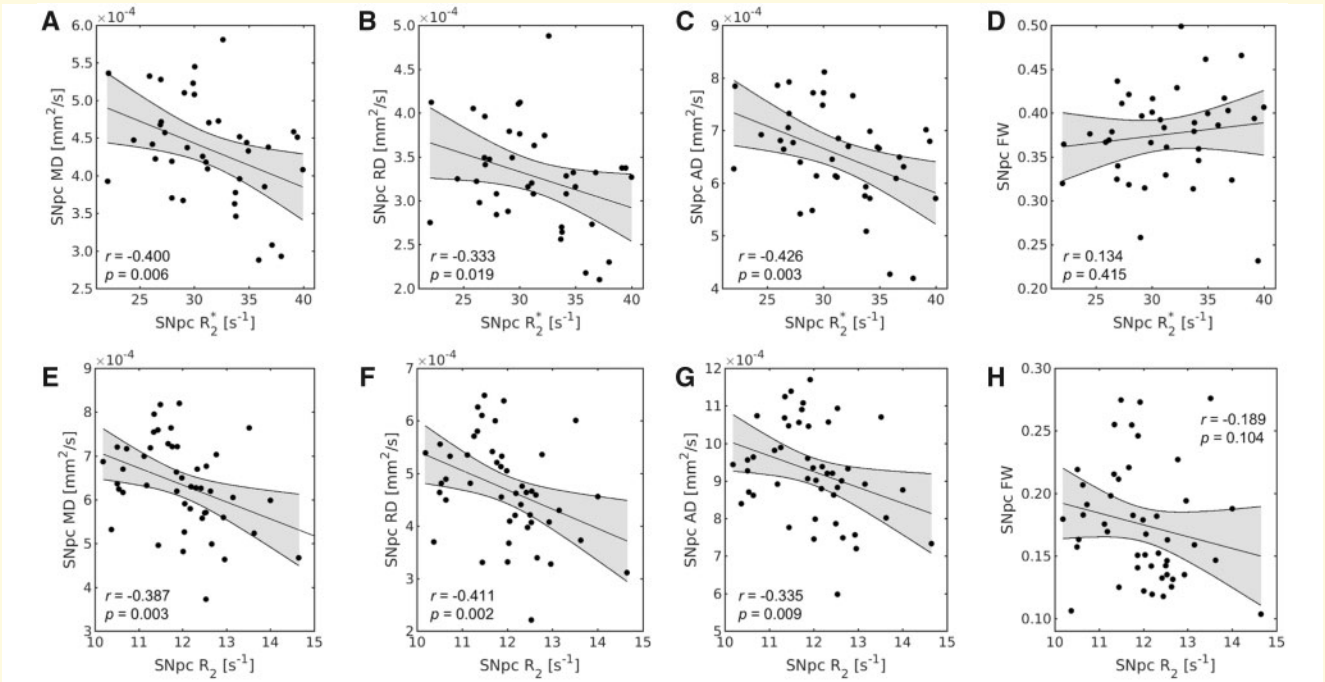

Figure 4 The relationship between iron and diffusivity in Parkinson's disease. Correlations between R_2* and diffusivity measures in the discovery cohort are shown in **A–D** and correlations between R_2 and diffusivity measures in the PPMI cohort are shown in **E–H**. Significant correlations between MD, RD and AD were seen in both cohorts while no significant correlations were observed for FW and iron in either cohort.

4.74×10^{-4} mm^2/s $\pm 1.04 \times 10^{-4}$ mm^2/s; $P = 0.295$; $t = -0.541$) or SNpc AD (Parkinson's: 9.41×10^{-4} mm^2/s $\pm 1.43 \times 10^{-4}$ mm^2/s; control: 9.72×10^{-4} mm^2/s $\pm 1.34 \times 10^{-4}$ mm^2/s; $P = 0.122$; $t = 1.171$). An increase in SNpc FW (Parkinson's: 0.19 ± 0.06; control: 0.16 ± 0.04; $P = 0.01$; $t = -2.379$) and SNpc R_2 (Parkinson's: $11.9 \pm 1.0\,s^{-1}$; control: $11.6 \pm 0.8\,s^{-1}$; $P = 0.023$; $t = -2.022$) was seen in the Parkinson's disease group compared to the control group. Group comparisons from both cohorts are summarized in Fig. 3.

The effect of Parkinson's disease-related iron deposition on diffusion signal in SNpc was assessed by correlating SNpc diffusion indices (MD, RD, AD and FW measures) with SNpc iron measures in both cohorts. SNpc R_2* was found to be negatively correlated with SNpc MD ($r = -0.400$; $P = 0.006$; $N = 39$), SNpc RD ($r = -0.333$; $P = 0.019$; $N = 39$) and SNpc AD ($r = -0.426$; $P = 0.003$; $N = 39$) in the Parkinson's disease group from the discovery cohort. Similarly, SNpc R_2 was found to be negatively correlated with SNpc MD ($r = -0.387$; $P = 0.003$; $N = 52$), SNpc RD ($r = -0.411$; $P = 0.002$; $N = 52$) and SNpc AD ($r = -0.335$; $P = 0.009$; $N = 52$) in the Parkinson's disease group from the PPMI cohort. However, no correlation was observed between iron measures and FW measures in the Parkinson's disease group of the discovery cohort (SNpc R_2* and SNpc FW: $r = 0.134$; $P = 0.415$; $N = 39$) or in the PPMI cohort (SNpc R_2 and SNpc FW: $r = -0.189$; $P = 0.104$; $N = 52$). These correlations are shown in Fig. 4. No correlations were observed between FW measures and iron measures in the control group of the discovery cohort (SNpc R_2* and SNpc FW: $r = 0.270$; $P = 0.156$; $N = 32$) or in the PPMI cohort (SNpc R_2 and SNpc FW: $r = -0.201$; $P = 0.145$; $N = 58$).

Diffusion measures of MD, RD and AD were found to be correlated with iron (R_2* or R_2) in both cohorts. Thus, to evaluate Parkinson's disease-related microstructural changes without the contribution of iron, we performed a *post hoc* ANCOVA on MD, RD and AD measures. In the discovery cohort, no significant effects were observed in the ANCOVA analysis for MD ($P = 0.868$; $F = 0.028$), RD ($P = 0.618$; $F = 0.251$) or AD ($P = 0.717$; $F = 0.132$). These results indicate that the group differences observed in nigral diffusivity in the discovery cohort were due to iron. No significant effects were seen in the ANCOVA analysis for MD ($P = 0.328$; $F = 0.965$), RD ($P = 0.310$; $F = 1.041$) or AD ($P = 0.432$; $F = 0.513$) in the PPMI cohort.

The Parkinson's disease group of the discovery cohort showed no correlation between ON UPDRS-II score and R_2* ($r = -0.059$; $P = 0.724$; $N = 39$), FW ($r = 0.010$; $P = 0.954$; $N = 39$), FA ($r = 0.116$; $P = 0.483$; $N = 39$) or MD ($r = -0.196$; $P = 0.233$; $N = 39$). Disease duration exhibited no association with R_2* ($r = 0.196$; $P = 0.239$; $N = 39$), FW ($r = 0.011$; $P = 0.953$; $N = 39$), FA ($r = 0.239$; $P = 0.143$; $N = 39$) or MD ($r = -0.073$; $P = 0.659$; $N = 39$) in the Parkinson's disease group of the discovery cohort. In the Parkinson's disease group of the PPMI cohort, no

association was seen between ON UPDRS-III score and R_2 ($r = -0.064$; $P = 0.683$; $N = 52$), FW ($r = 0.121$; $P = 0.428$; $N = 52$), FA ($r = 0.065$; $P = 0.673$; $N = 52$) or MD ($r = 0.054$; $P = 0.725$; $N = 52$). No significant correlation was found between disease duration and R_2 ($r = -0.099$; $P = 0.497$; $N = 52$), FW ($r = -0.008$; $P = 0.954$; $N = 52$), FA ($r = -0.035$; $P = 0.807$; $N = 52$) or MD ($r = -0.009$; $P = 0.947$; $N = 52$) in the Parkinson's disease group of the PPMI cohort.

In the discovery cohort mean SNpc R_2^* outperformed SNpc diffusion indices as a diagnostic imaging marker. The area under the receiver operating characteristic (ROC) curve (AUC) for mean SNpc R_2^* was 0.813 [standard error (SE) = 0.056; 95% confidence interval (95% CI): 0.704–0.922; $P < 10^{-4}$). The AUC for mean SNpc FW was 0.600 (SE = 0.068; 95% CI: 0.527–0.792; $P = 0.025$). In the PPMI cohort SNpc R_2 and SNpc FW performed similarly as diagnostic imaging markers. The AUC for SNpc R_2 was 0.609 (SE = 0.06; 95% CI: 0.497–0.721; $P = 0.05$) and SNpc FW was 0.611 (SE = 0.05; 95% CI: 0.502–0.719; $P = 0.05$). ROC curves for both cohorts are shown in Fig. 5.

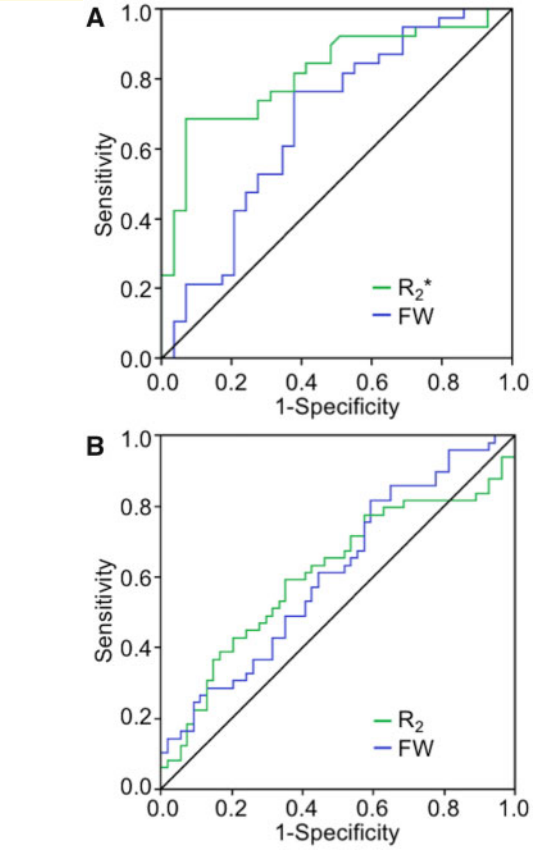

Figure 5 Receiver operator characteristic analyses of nigral iron and FW. (**A**) Receiver operator characteristic curves for the discovery cohort. (**B**) Receiver operator characteristic curves for the PPMI cohort.

Discussion

This study examines Parkinson's disease-related changes in SNpc microstructure and iron content in two cohorts with similar clinical characteristics. Parkinson's disease patients experience a loss of melanized neurons in SNpc[2,3] and elevated levels of non-heme ferric iron (Fe^{3+}) are observed alongside the loss of melanized neurons.[4–6] Elevated iron levels should impact MRI images by causing larger transverse relaxation rates while reductions in melanized neurons should cause increases in MRI measures sensitive to FW, as this compartment would be increased in areas of neuronal loss. In line with histological findings, we observed increases in iron measures and FW measures in SNpc the Parkinson's disease group of both cohorts. However, diffusivity measures from the single-compartment DTI model (FA, MD and RD) were found to be inconsistent Parkinson's disease diagnostic markers, with the discovery cohort showing altered SNpc diffusivity in the Parkinson's disease group, while no group differences were seen with these DTI markers in SNpc in the PPMI cohort. All single-compartment diffusion markers (FA, MD, RD and AD) were found to be significantly correlated with iron, whereas the two-compartment model diffusion measure, FW, did not correlate significantly with iron. Together, these results suggest that variability in tissue iron levels may impact diffusion-MRI results with single-compartment DTI measures but not FW from the bi-compartment model.

Neuromelanin granules in substantia nigra chelate iron.[53,54] Sequestered iron may be released when neuromelanin granules are phagocytosed and degraded after the loss of melanized neurons. Increases in transverse relaxation rates were seen in SNpc of the discovery cohort (R_2^*) and the PPMI cohort (R_2), indicating iron is being deposited in SNpc of Parkinson's disease patients. These results agree with earlier studies that found an increase in mean SNpc R_2^* of Parkinson's disease patients[51,55] and those reporting an increase in mean nigral transverse relaxation rates in regions drawn in the T_2-weighted substantia nigra.[11,12,27–33]

Measures sensitive to the FW compartment in SNpc were found to increase in the Parkinson's disease group of both cohorts. These results are consistent with earlier work reporting increased nigral FW of Parkinson's disease patients.[20,21,23,25,56,57] The FW compartment represents extracellular water molecules (i.e. molecules unhindered by cellular environment) within a voxel.[46,58] Increases in the FW compartment are generally interpreted as a reduction of SNpc neuronal density.[21,23] Since the ROI used to define SNpc was derived from neuromelanin-sensitive images, the increase in the FW compartment of the Parkinson's disease group of both cohorts may reflect a loss of melanized neurons in SNpc.

An increase of the FW compartment should yield an increase in diffusivity from the single-compartment model.

However, a reduction in SNpc diffusivity was observed in the Parkinson's disease group of the discovery cohort and this agrees with an earlier study reporting reduced SNpc diffusivity in a similar SNpc ROI.[15] This reduction in diffusivity may be due to the influence of iron as higher iron measures have been observed to negatively bias nigral diffusivity in older adults[34] or striatal diffusivity in older adults[35] or patients with Huntington's disease.[52] Local magnetic field gradients from iron deposits produce cross terms with diffusion encoding gradients and reduce the apparent diffusion coefficient.[59,60] In agreement with this model, we observed negative correlations between mean SNpc R_2* and SNpc diffusivity in the Parkinson's disease group of the discovery cohort.

Mean SNpc single-compartment diffusivity measures in the Parkinson's disease group of the PPMI cohort were negatively correlated with mean SNpc R_2, but no group differences in single-compartment diffusivity measures were observed. This is in agreement with an earlier study, which found no difference in nigral diffusivity measures between Parkinson's disease and control groups.[61] The lack of a disease effect for single-compartment diffusion markers in these studies may be attributed to two competing influences: a reduction in melanized neurons, which tends to drive diffusivity up and FA down, and iron deposition, which tends to drive diffusivity down and FA up. In some cases, these competing effects may offset and reduce the effect size. These competing effects may partially explain variability observed in earlier diffusion studies examining nigral DTI metrics where studies have reported lower nigral FA[10–13,15] or no difference in nigral FA.[8,16–19]

The ROC analysis found AUC of nigral R_2* to be comparable to previously published diagnostic markers examining nigral tissue composition,[62–67] which have AUCs between 0.7 and 0.9. However, AUC for nigral FW in both cohorts was significantly below AUCs reported in other studies.[23,68] The discrepancy in performance of FW imaging markers may be related to ROI selection. We used the entire SNpc was used as an ROI in the AUC analysis while earlier studies reported AUC in SNpc subregions with ROIs placed in the posterior SNpc.[20,21,23,69] Nigrosome-1, the SNpc subregion that experiences the greatest loss of melanized neurons, is located in the posterior portion of SNpc[49] and posterior SNpc ROIs likely capture degeneration in nigrosome-1, whereas the entire SNpc ROI will contain nigrosome-1 as well as other regions that lose fewer melanized neurons.

The study has several caveats. First, only a subset of the PPMI cohort was used in the diffusion and iron analyses. This was due to inconsistent R_2 and DTI scan parameters at several imaging sites. Second, Parkinson's disease-related iron deposition is expected to reduce signal-to-noise ratios in SNpc. This deposition should increase noise and may corrupt diffusion measures in the discovery and PPMI cohorts. Reduced signal-to-noise ratios will positively bias AD and FA while negatively biasing RD.[70] We speculate that the effect of noise is minimal in both cohorts since correlations of similar strength are seen between iron metrics and both RD and AD. Third, monopolar diffusion encoding gradients were applied in both cohorts. Bipolar diffusion encoding gradients may be less sensitive to iron deposits.[71] However, a recent study found R_2* negatively biases diffusivity[34] and additional work is needed to fully assess the contribution of iron on diffusivity in grey matter structures.

In this work, Parkinson's disease-related changes in SNpc microstructure and iron content were examined in two cohorts with similar clinical characteristics. Measures sensitive to FW and iron content were found to increase in SNpc of the Parkinson's disease group in both cohorts. However, diffusion markers derived from the single-compartment model (i.e. MD, RD, AD and FA) were not replicated across cohorts. The variability of metrics derived from the single-compartment model may be attributed to competing influences of iron content[34,35,52] and FW on the diffusion signal, the placement of ROIs outside SNpc,[15,17] or a combination of these factors. In contrast to SNpc diffusivity, no association was found between SNpc FW and SNpc iron measures in either cohort. This insensitivity to iron, coupled with consistent observations of increased nigral FW from this study and earlier studies,[20,21,23,25,56,57] suggests the FW compartment of bi-compartment diffusion models should be used in lieu of diffusivity measures derived from the single-compartment model to study SNpc.

Funding

This work was supported by grants MJFF-010556 and MJFF-010854 from the Michael J. Fox Foundation for Parkinson's Research (D.E.H., J.L. and X.H.), 1K23NS105944-01A1 (D.E.H.) from the National Institutes of Health/National Institute of Neurological Diseases and Stroke, and the American Parkinson's Disease Foundation Center for Advanced Research at Emory University (D.E.H.). PPMI—a public–private partnership—is funded by the Michael J. Fox Foundation for Parkinson's Research and funding partners, including (list the full names of all of the PPMI funding partners found at www.ppmi-info.org/fundingpartners).

Competing interests

The authors report no competing interests.

References

1. Kowal SL, Dall TM, Chakrabarti R, Storm MV, Jain A. The current and projected economic burden of Parkinson's disease in the United States. *Mov Disord*. 2013;28(3):311–318.

2. Damier P, Hirsch EC, Agid Y, Graybiel AM. The substantia nigra of the human brain. II. Patterns of loss of dopamine-containing neurons in Parkinson's disease. *Brain*. 1999;122 (8):1437–1448.
3. Fearnley JM, Lees AJ. Ageing and Parkinson's disease: substantia nigra regional selectivity. *Brain*. 1991;114 (5):2283–2301.
4. Dexter DT, Carayon A, Javoy-Agid F, et al. Alterations in the levels of iron, ferritin and other trace metals in Parkinson's disease and other neurodegenerative diseases affecting the basal ganglia. *Brain*. 1991;114 (4):1953–1975.
5. Dexter DT, Wells FR, Agid F, et al. Increased nigral iron content in postmortem parkinsonian brain. *Lancet*. 1987;2(8569):1219–1220.
6. Wypijewska A, Galazka-Friedman J, Bauminger ER, et al. Iron and reactive oxygen species activity in parkinsonian substantia nigra. *Parkinsonism Relat Disord*. 2010;16(5):329–333.
7. Beaulieu C. The basis of anisotropic water diffusion in the nervous system - a technical review. *NMR Biomed*. 2002;15(7-8):435–455.
8. Aquino D, Contarino V, Albanese A, et al. Substantia nigra in Parkinson's disease: A multimodal MRI comparison between early and advanced stages of the disease. *Neurol Sci*. 2014;35(5): 753–758.
9. Blain CR, Barker GJ, Jarosz JM, et al. Measuring brain stem and cerebellar damage in parkinsonian syndromes using diffusion tensor MRI. *Neurology*. 2006;67(12):2199–2205.
10. Chan LL, Rumpel H, Yap K, et al. Case control study of diffusion tensor imaging in Parkinson's disease. *J Neurol Neurosurg Psychiatry*. 2007;78(12):1383–1386.
11. Du G, Lewis MM, Styner M, et al. Combined R2 * and diffusion tensor imaging changes in the substantia nigra in Parkinson's disease. *Mov Disord*. 2011;26(9):1627–1632.
12. Peran P, Cherubini A, Assogna F, et al. Magnetic resonance imaging markers of Parkinson's disease nigrostriatal signature. *Brain*. 2010;133(11):3423–3433.
13. Vaillancourt DE, Spraker MB, Prodoehl J, et al. High-resolution diffusion tensor imaging in the substantia nigra of de novo Parkinson disease. *Neurology*. 2009;72(16):1378–1384.
14. Lenfeldt N, Larsson A, Nyberg L, Birgander R, Forsgren L. Fractional anisotropy in the substantia nigra in Parkinson's disease: A complex picture. *Eur J Neurol*. 2015;22(10):1408–1414.
15. Langley J, Huddleston DE, Merritt M, et al. Diffusion tensor imaging of the substantia nigra in Parkinson's disease revisited. *Hum Brain Mapp*. 2016;37(7):2547–2556.
16. Menke RA, Scholz J, Miller KL, et al. MRI characteristics of the substantia nigra in Parkinson's disease: A combined quantitative T1 and DTI study. *NeuroImage*. 2009;47(2):435–441.
17. Schwarz ST, Abaei M, Gontu V, Morgan PS, Bajaj N, Auer DP. Diffusion tensor imaging of nigral degeneration in Parkinson's disease: A region-of-interest and voxel-based study at 3 T and systematic review with meta-analysis. *Neuroimage Clin*. 2013;3: 481–488.
18. Focke NK, Helms G, Pantel PM, et al. Differentiation of typical and atypical Parkinson syndromes by quantitative MR imaging. *AJNR Am J Neuroradiol*. 2011;32(11):2087–2092.
19. Ziegler E, Rouillard M, Andre E, et al. Mapping track density changes in nigrostriatal and extranigral pathways in Parkinson's disease. *Neuroimage*. 2014;99:498–508.
20. Guttuso T Jr, Bergsland N, Hagemeier J, Lichter DG, Pasternak O, Zivadinov R. Substantia nigra free water increases longitudinally in Parkinson disease. *AJNR Am J Neuroradiol*. 2018;39(3):479–484.
21. Ofori E, Pasternak O, Planetta PJ, et al. Increased free water in the substantia nigra of Parkinson's disease: A single-site and multi-site study. *Neurobiol Aging*. 2015;36(2):1097–1104.
22. Burciu RG, Ofori E, Archer DB, et al. Progression marker of Parkinson's disease: A 4-year multi-site imaging study. *Brain*. 2017;140(8):2183–2192.
23. Planetta PJ, Ofori E, Pasternak O, et al. Free-water imaging in Parkinson's disease and atypical parkinsonism. *Brain*. 2016;139(Pt 2):495–508.
24. Wang JJ, Lin WY, Lu CS, et al. Parkinson disease: Diagnostic utility of diffusion kurtosis imaging. *Radiology*. 2011;261(1):210–217.
25. Kamagata K, Hatano T, Okuzumi A, et al. Neurite orientation dispersion and density imaging in the substantia nigra in idiopathic Parkinson disease. *Eur Radiol*. 2016;26(8):2567–2577.
26. Langley J, He N, Huddleston DE, et al. Reproducible detection of nigral iron deposition in 2 Parkinson's disease cohorts. *Mov Disord*. 2019;34(3):416–419.
27. Baudrexel S, Nurnberger L, Rub U, et al. Quantitative mapping of T1 and T2 * discloses nigral and brainstem pathology in early Parkinson's disease. *Neuroimage*. 2010;51(2):512–520.
28. Gorell JM, Ordidge RJ, Brown GG, Deniau JC, Buderer NM, Helpern JA. Increased iron-related MRI contrast in the substantia nigra in Parkinson's disease. *Neurology*. 1995;45(6):1138–1143.
29. Graham JM, Paley MN, Grunewald RA, Hoggard N, Griffiths PD. Brain iron deposition in Parkinson's disease imaged using the PRIME magnetic resonance sequence. *Brain*. 2000;123(Pt 12): 2423–2431.
30. Kosta P, Argyropoulou MI, Markoula S, Konitsiotis S. MRI evaluation of the basal ganglia size and iron content in patients with Parkinson's disease. *J Neurol*. 2006;253(1):26–32.
31. Martin WR, Wieler M, Gee M. Midbrain iron content in early Parkinson disease: A potential biomarker of disease status. *Neurology*. 2008;70(16):1411–1417.
32. Wallis LI, Paley MN, Graham JM, et al. MRI assessment of basal ganglia iron deposition in Parkinson's disease. *J Magn Reson Imaging*. 2008;28(5):1061–1067.
33. Ryvlin P, Broussolle E, Piollet H, Viallet F, Khalfallah Y, Chazot G. Magnetic resonance imaging evidence of decreased putamenal iron content in idiopathic Parkinson's disease. *Arch Neurol*. 1995; 52(6):583–588.
34. Langley J, Hussain S, Flores JJ, Bennett IJ, Hu X. Characterization of age-related microstructural changes in locus coeruleus and substantia nigra pars compacta. *Neurobiol Aging*. 2020;87:89–97.
35. Pfefferbaum A, Adalsteinsson E, Rohlfing T, Sullivan EV. Diffusion tensor imaging of deep gray matter brain structures: Effects of age and iron concentration. *Neurobiol Aging*. 2010; 31(3):482–493.
36. Sasaki M, Shibata E, Tohyama K, et al. Neuromelanin magnetic resonance imaging of locus ceruleus and substantia nigra in Parkinson's disease. *Neuroreport*. 2006;17(11):1215–1218.
37. Chen X, Huddleston DE, Langley J, et al. Simultaneous imaging of locus coeruleus and substantia nigra with a quantitative neuromelanin MRI approach. *Magn Reson Imaging*. 2014;32(10): 1301–1306.
38. Schwarz ST, Rittman T, Gontu V, Morgan PS, Bajaj N, Auer DP. T1-Weighted MRI shows stage-dependent substantia nigra signal loss in Parkinson's disease. *Mov Disord*. 2011;26(9):1633–1638.
39. Langley J, Huddleston DE, Chen X, Sedlacik J, Zachariah N, Hu X. A multicontrast approach for comprehensive imaging of substantia nigra. *Neuroimage*. 2015;112:7–13.
40. Postuma RB, Berg D, Stern M, et al. MDS clinical diagnostic criteria for Parkinson's disease. *Mov Disord*. 2015;30(12):1591–1601.
41. Berardelli A, Wenning GK, Antonini A, et al. EFNS/MDS-ES/ENS [corrected] recommendations for the diagnosis of Parkinson's disease. *Eur J Neurol*. 2013;20(1):16–34.
42. Andersson JLR, Skare S, Ashburner J. How to correct susceptibility distortions in spin-echo echo-planar images: Application to diffusion tensor imaging. *NeuroImage*. 2003;20(2):870–888.
43. Jenkinson M, Bannister P, Brady M, Smith S. Improved optimization for the robust and accurate linear registration and motion correction of brain images. *NeuroImage*. 2002;17(2):825–841.
44. Jenkinson M, Smith S. A global optimisation method for robust affine registration of brain images. *Med Image Anal*. 2001;5(2): 143–156.
45. Smith SM, Jenkinson M, Woolrich MW, et al. Advances in functional and structural MR image analysis and implementation as FSL. *NeuroImage*. 2004;23:S208–S219.

46. Pasternak O, Sochen N, Gur Y, Intrator N, Assaf Y. Free water elimination and mapping from diffusion MRI. *Magn Reson Med*. 2009;62(3):717–730.
47. Garyfallidis E, Brett M, Amirbekian B, et al.; Dipy Contributors. Dipy, a library for the analysis of diffusion MRI data. *Front Neuroinform*. 2014;8:8.
48. Smith SM. Fast robust automated brain extraction. *Hum Brain Mapp*. 2002;17(3):143–155.
49. Langley J, Huddleston DE, Crosson B, Song DD, Factor SA, Hu X. Multimodal assessment of nigrosomal degeneration in Parkinson's disease. *Parkinsonism Relat Disord*. 2020;80: 102–107.
50. Woolrich MW, Jbabdi S, Patenaude B, et al. Bayesian analysis of neuroimaging data in FSL. *NeuroImage*. 2009;45(Suppl 1): S173–S186.
51. He N, Langley J, Huddleston DE, et al. Increased iron-deposition in lateral-ventral substantia nigra pars compacta: A promising neuroimaging marker for Parkinson's disease. *Neuroimage Clin*. 2020;28:102391.
52. Syka M, Keller J, Klempí J, et al. Correlation between relaxometry and diffusion tensor imaging in the globus pallidus of Huntington's disease patients. *PLoS One*. 2015;10(3):e0118907.
53. Zecca L, Casella L, Albertini A, et al. Neuromelanin can protect against iron-mediated oxidative damage in system modeling iron overload of brain aging and Parkinson's disease. *J Neurochem*. 2008;106(4):1866–1875.
54. Sulzer D, Cassidy C, Horga G, et al. Neuromelanin detection by magnetic resonance imaging (MRI) and its promise as a biomarker for Parkinson's disease. *NPJ Parkinsons Dis*. 2018;4:11.
55. He N, Ghassaban K, Huang P, et al. Imaging iron and neuromelanin simultaneously using a single 3D gradient echo magnetization transfer sequence: Combining neuromelanin, iron and the nigrosome-1 sign as complementary imaging biomarkers in early stage Parkinson's disease. *Neuroimage*. 2021;230:117810.
56. Arribarat G, Pasternak O, De Barros A, Galitzky M, Rascol O, Péran P. Substantia nigra locations of iron-content, free-water and mean diffusivity abnormalities in moderate stage Parkinson's disease. *Parkinsonism Relat Disord*. 2019;65:146–152.
57. Ofori E, Krismer F, Burciu RG, et al. Free water improves detection of changes in the substantia nigra in parkinsonism: A multisite study. *Mov Disord*. 2017;32(10):1457–1464.
58. Zhang H, Schneider T, Wheeler-Kingshott CA, Alexander DC. NODDI: Practical *in vivo* neurite orientation dispersion and density imaging of the human brain. *Neuroimage*. 2012;61(4): 1000–1016.
59. Zhong J, Kennan RP, Gore JC. Effects of susceptibility variations on NMR measurements of diffusion. *J Magn Reson*. 1991;95(2): 267–280.
60. Novikov DS, Reisert M, Kiselev VG. Effects of mesoscopic susceptibility and transverse relaxation on diffusion NMR. *J Magn Reson*. 2018;293:134–144.
61. Schuff N, Wu IW, Buckley S, et al. Diffusion imaging of nigral alterations in early Parkinson's disease with dopaminergic deficits. *Mov Disord*. 2015;30(14):1885–1892.
62. Cheng Z, He N, Huang P, et al. Imaging the Nigrosome 1 in the substantia nigra using susceptibility weighted imaging and quantitative susceptibility mapping: An application to Parkinson's disease. *Neuroimage Clin*. 2020;25:102103.
63. Li G, Zhai G, Zhao X, et al. 3D texture analyses within the substantia nigra of Parkinson's disease patients on quantitative susceptibility maps and R2(*) maps. *Neuroimage*. 2019;188:465–472.
64. Ariz M, Abad RC, Castellanos G, et al. Dynamic atlas-based segmentation and quantification of neuromelanin-rich brainstem structures in Parkinson disease. *IEEE Trans Med Imaging*. 2019; 38(3):813–823.
65. Shinde S, Prasad S, Saboo Y, et al. Predictive markers for Parkinson's disease using deep neural nets on neuromelanin sensitive MRI. *Neuroimage Clin*. 2019;22:101748.
66. Huddleston DE, Langley J, Sedlacik J, Boelmans K, Factor SA, Hu XP. *In vivo* detection of lateral-ventral tier nigral degeneration in Parkinson's disease. *Hum Brain Mapp*. 2017;38(5):2627–2634.
67. Schwarz ST, Xing Y, Tomar P, Bajaj N, Auer DP. *In vivo* assessment of brainstem depigmentation in Parkinson disease: Potential as a severity marker for multicenter studies. *Radiology*. 2016; 283(3):789–798.
68. Zhou L, Li G, Zhang Y, et al. Increased free water in the substantia nigra in idiopathic REM sleep behaviour disorder. *Brain*. 2021; 144(5):1488–1497.
69. Yang J, Archer DB, Burciu RG, et al. Multimodal dopaminergic and free-water imaging in Parkinson's disease. *Parkinsonism Relat Disord*. 2019;62:10–15.
70. Anderson AW. Theoretical analysis of the effects of noise on diffusion tensor imaging. *Magn Reson Med*. 2001;46(6):1174–1188.
71. Fujiwara S, Uhrig L, Amadon A, Jarraya B, Le Bihan D. Quantification of iron in the non-human primate brain with diffusion-weighted magnetic resonance imaging. *Neuroimage*. 2014; 102(2):789–797.